
MIPANET: OPTIMIZING RGB-D SEMANTIC SEGMENTATION THROUGH MULTI-MODAL INTERACTION AND POOLING ATTENTION

Shuai Zhang

Faculty of Information Engineering and Automation
Kunming University of Science and Technology
Kunming, 650500 Yunnan, PR China
zhangshuai2@stu.kust.edu.cn

Minghong Xie

Key Laboratory of Artificial Intelligence in Yunnan Province
Kunming University of Science and Technology
Kunming, 650500 Yunnan, PR China
minghongxie@qq.com

November 21, 2023

ABSTRACT

Semantic segmentation of RGB-D images involves understanding the appearance and spatial relationships of objects within a scene, which requires careful consideration of various factors. However, in indoor environments, the simple input of RGB and depth images often results in a relatively limited acquisition of semantic and spatial information, leading to suboptimal segmentation outcomes. To address this, we propose the Multi-modal Interaction and Pooling Attention Network (MIPANet), a novel approach designed to harness the interactive synergy between RGB and depth modalities, optimizing the utilization of complementary information. Specifically, we incorporate a Multi-modal Interaction Fusion Module (MIM) into the deepest layers of the network. This module is engineered to facilitate the fusion of RGB and depth information, allowing for mutual enhancement and correction. Additionally, we introduce a Pooling Attention Module (PAM) at various stages of the encoder. This module serves to amplify the features extracted by the network and integrates the module's output into the decoder in a targeted manner, significantly improving semantic segmentation performance. Our experimental results demonstrate that MIPANet outperforms existing methods on two indoor scene datasets, NYUDv2 and SUN-RGBD, underscoring its effectiveness in enhancing RGB-D semantic segmentation.

1 Introduction

In recent years, Convolutional Neural Networks (CNN) have been widely used in image semantic segmentation, and more and more high-performance models have gradually replaced the traditional semantic segmentation methods. With the introduction of Fully Convolutional Neural Networks [1, 2], which show great potential in semantic segmentation tasks, many researchers have proposed improved semantic segmentation models based on this way. Nevertheless, semantic segmentation remains a formidable challenge in some indoor environments, given the intricacies such as variations in illumination and mutual occlusion between objects.

With the advent of depth sensors and depth cameras [3], The research on images is not limited to RGB colour images, but the research on RGB-depth (RGB-D) images containing Depth information. RGB images can provide appearance information such as the colour and texture of objects, in contrast, depth images can provide three-dimensional geometry information of objects, which is missing in RGB images and is desired for indoor scenes. [4, 5] simply splice RGB

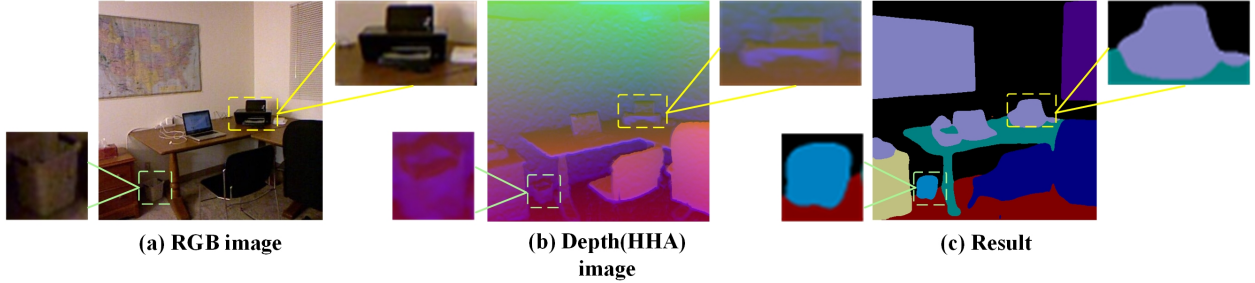


Figure 1: Enhance segmentation accuracy by leveraging depth features within our MIPANet. The prediction result can accurately distinguish the trash can and printer from the background.

features and depth features to form a four-channel input, improving the accuracy of semantic segmentation. [6] further encode the depth information into HHA features and then input the colour features and HHA features into two parallel CNNs to predict the probability maps of two semantic segmentations respectively and fuse them in the last layer of the network as the final segmentation result. Nonetheless, though the above methods have achieved good results in the task of RGB-D semantic segmentation, however, most RGB-D semantic segmentation [7, 8, 9, 10] simply merges RGB features and depth features by concatenation or summation. As a result, the information differences between the modes cannot be solved effectively, which will cause the convolutional neural network not to fully use the complementary information between them, resulting in object and background confusion. For example, The printer and trash bin in Fig. 1 (a) are prone to be inaccurately assimilated into the background.

To solve the above problems, we propose an RGB-D semantic segmentation of the Indoor Scene network, MIPANet. Fig. 2 illustrates the overall structure of the network. The network is an encoder-decoder architecture, including two innovative feature fusion modules: The multi-modal Interaction Fusion Module and the Pooling Attention Module. This paper integrates the two fusion modules into an encoder-decoder architecture. The encoder is composed of two identical CNN branches, each specifically designed for extracting RGB features and depth features, respectively. In this study, RGB and depth features are extracted and fused incrementally across various network levels, capitalising on spatial disparities and semantic interdependencies among multimodal features to enhance the effectiveness of semantic segmentation. In our PAM, we use adaptive averaging instead of global averaging, which approach not only allows for flexible adjustment of the output size but also preserves more spatial information, facilitating enhanced extraction of depth features. And in MIM, we obtain two sets of QKV for different modalities and perform calculations using the QK from one set and V from the other. This achieves information interaction between the RGB and depth modalities. This paper’s main contributions can be summarized as follows:

- Introduced an end-to-end multi-modal fusion network, MIPANet, incorporating multi-modal interaction and pooling attention. This innovative approach optimizes integrating complementary information from RGB and depth features, effectively tackling the semantic segmentation challenges posed by RGB-D indoor scenes.
- Presented two cross-modal feature fusion methods. Within the MIM, a cross-modal feature interaction and fusion mechanism were developed. RGB and depth features are collaboratively optimized using attention masks to extract partially detailed features. Conversely, PAM integrates intermediate layer features into the convolutional neural network, enhancing feature extraction and supporting the decoder in upsampling and recovery.
- Experimental results confirm the effectiveness of our proposed RGB-D semantic segmentation network in accurately handling indoor images in complex scenarios. The model demonstrated superior semantic segmentation performance compared to other methods on the publicly available NYUv2 and SUN RGB-D datasets.

2 Related Work

In this section, we provide a comprehensive review of three parts, (1) RGB-D semantic segmentation, (2) attention module, and (3) interaction module.

RGB-D Semantic Segmentation. With the widespread application of depth sensors and depth cameras in the field of depth estimation [11, 9, 12, 13], people can obtain the depth information of the scene more conveniently, and the research on the image is no longer limited to a single RGB image. RGB-D semantic segmentation task is to efficiently integrate RGB features and depth features to improve segmentation accuracy, especially in some indoor scenes. Couprie et al. [4] proposed an early fusion approach, which simply concatenates the RGB and depth channels of an image as

a four-channel input to the convolutional neural network. Wang et al. [6] separately input RGB features and HHA features into two CNNs for prediction and perform fusion in the final stage of the network, and [14] introduced an encoding-decoding network, employing a dual-branch RGB encoder to extract features separately from RGB images and depth images. The studies mentioned above employed equal-weight concatenation or summation operations to fuse RGB features and depth features, without fully leveraging the complementary information between different modalities. In recent years, some research has proposed more effective strategies for RGB-D feature fusion. Hu et al. [15] utilised a three-branch encoder that includes RGB, Depth, and Fusion branches, efficiently collecting features without breaking the original RGB and deep inference branches. Seichter et al. [16] have presented an efficient RGB-D segmentation approach, which is characterised by two enhanced ResNet-based encoders utilising an attention-based fusion for incorporating depth information. However, these methods did not fully exploit the differential information between the two modalities and the intermediate-level features extracted by the convolutional network.

Attention Module. In recent years, attention [17, 18, 19, 20, 21, 22] has been widely used in computer vision and other fields. Vaswani et al. [17] proposed the self-attention mechanism, which has had a profound impact on the design of the deep learning model. Fu et al. [19] proposed DANet, which can adaptively integrate local features and their global dependencies. Wang et al. [23] utilised spatial attention in an image classification model. Through the backpropagation of a convolutional neural network, they adaptively learned spatial attention masks, allowing the model to focus on the significant regions of the image. SENet [24] have proposed channel attention which adaptively learns the importance of each feature channel through a neural network. Woo et al. [22] incorporates two attention modules that concurrently capture both channel-wise and spatial relationships. ECA-Net [25] introduces a straightforward and efficient "local" channel attention mechanism, aiming to minimize computational overhead. MFC [26] introduced a multi-frequency domain attention module aimed at capturing information across different frequency domains. Similarly, CAMNet [2] proposed a contrastive attention module designed to amplify local saliency. Building upon this foundation, Huang et al. [27] proposed a cross-attention module that consolidates contextual information both horizontally and vertically, which can gather contextual information from all pixels. These methods have demonstrated significant potential in single-mode feature extraction. To effectively leverage the complementary information between different modalities, this paper introduces a Pooling Attention module that learns the differential information between two distinct modalities and fully exploits the intermediate-level features in the convolutional network, as well as long-range semantic dependencies between modalities.

Interaction Module. With the development of sensor technology, different types of sensors can provide a variety of modal information for semantic segmentation tasks, to achieve information interaction [28, 29, 30, 31, 32] between RGB mode and other modes. The interaction between RGB and infrared modalities enhanced the effectiveness of semantic segmentation in RGB-T scenarios. Xiang et al. [33] used a single-shot polarization sensor to build the first RGB-P dataset, incorporated polarization sensing to obtain supplementary information, and improved the accuracy of segmentation for many categories, especially those with polarization characteristics, such as glass. HPGN [34] proposes a novel pyramid graph network targeting features, which is closely connected behind the backbone network to explore multi-scale spatial structural features. GiT [35] proposes a structure where graphs and transformers interact constantly, enabling close collaboration between global and local features for vehicle re-identification. Zhuang et al. [36] propose a network consisting of a two-streams (LiDAR stream and camera stream), which extract features from two modes respectively to realize information interaction between RGB and LIDAR modes. It is feasible to improve the result of semantic segmentation by information interaction between different modes and RGB mode.

3 Propose Methods

3.1 Overview

Fig. 2 illustrates the overall structure of the network. The network is an encoder-decoder architecture that utilizes skip connections to propagate information between the encoding and decoding layers. Specifically, the encoder consists of a dual-branch convolutional network, each dedicated to extracting RGB features and depth features. We use two pre-trained ResNet50 models as the baseline, removing the final global average pooling layer and fully connected layers. Then, we employ a decoder to progressively upsample the features, gradually restoring image resolution.

In this paper, the network model introduces two feature Fusion modules: the Multi-modal Interaction Fusion Module and the Pooling Attention Module. Specifically, the first three multi-level RGB features (ResL1-ResL3) and depth features (ResL1-ResL3) of the ResNet encoder are fed into the PAM module, and the pooled attention weighting operations are performed on the RGB features and depth features respectively to obtain RGB' and Dep' . Then we add the two features to get P' , which contains rich spatial location information. Furthermore, the final RGB and depth features from the ResNet(ResL4) encoder are fed into the MIM module to capture the complementary information within these two modalities. Then, the output features of the MIM module are input to the decoder. In each upsampling

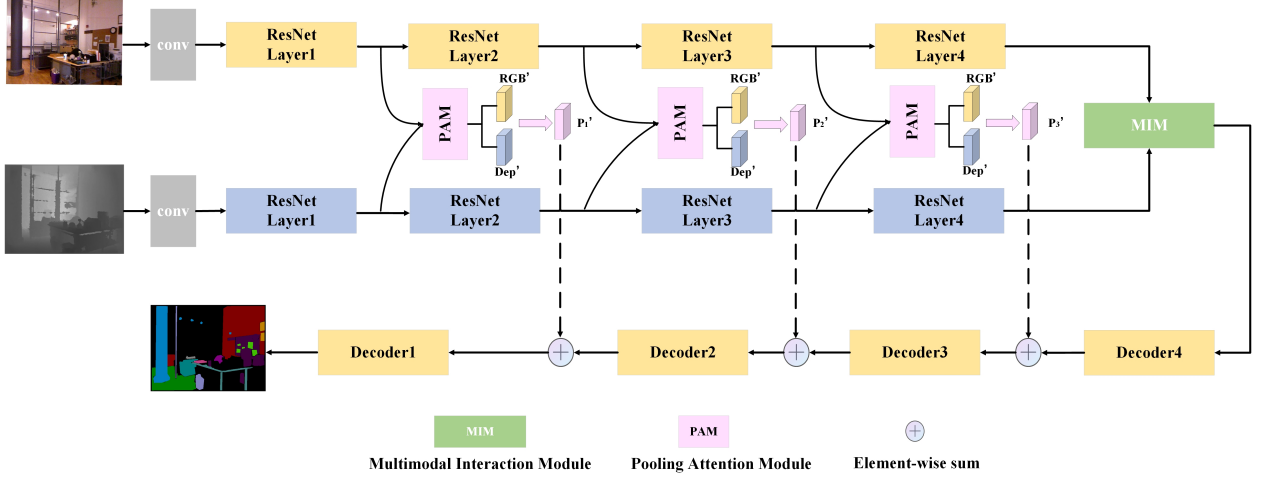


Figure 2: Multi-modal Interaction And Pooling Attention (MIPA) Network architecture. The two branches of the ResNet are respectively dedicated to extracting RGB features and depth features. Each PAM at different levels of the network generates two weight-unshared features: RGB features denoted as RGB' and depth features denoted as Dep' . After the Element-wise sum, we get P'_i , where i denotes the level of the network. MIM receives RGB features and depth features from the 4th layer and feeds the fusion result into the decoder.

layer, there are two 3×3 convolutional layers, each followed by batch normalization (BN) and ReLU activation. Each upsampling layer doubles the feature spatial dimensions while reducing the number of channels by half.

The following two subsections will provide detailed introductions to the MIM and PAM modules within the network model, respectively.

3.2 Pooling Attention Module

Within the low-level features extracted by the convolutional neural network, we capture the fundamental attributes of the input image. These low-level features are critical in modelling the image's foundational characteristics. However, they tend to lack higher-level semantic information, such as object shapes and categories. At the same time, while up-sampling in the decoding layer, there is a risk of losing certain semantic information as the image resolution increases. To address this, we introduce the PAM module to elevate the performance of these low-level features and employ it to compensate for the information loss during the up-sampling process as shown in Fig. 3.

Assuming the input feature maps $\mathbf{X} = [X_i, X_j] \in \mathbb{R}^{c \times h \times w}$, where X_i and X_j denote the RGB feature or Depth feature. We first apply Adaptive average pooling, to have the output $\mathbf{A} \in \mathbb{R}^{c \times 1 \times 1}$, where c denotes the number of channels, h, w denote the height and width of feature maps respectively. The k ($k \in [1, c]$) of \mathbf{A} can be expressed as:

$$Scale_h = h'/h \quad (1)$$

$$Scale_w = w'/w \quad (2)$$

Where $Scale_h$ and $Scale_w$ denote the scaling factors, h, w represent the height and width of the input feature map, and h', w' represent the height and width of the output feature map.

$$\mathbf{A} = \frac{1}{Scale_h * Scale_w} \sum_i^h \sum_j^w \mathbf{X}(i, j) \quad (3)$$

The scaling factor is used to consider the size difference between input and output. Then \mathbf{A} is reorganized by a 1×1 convolution layer with the same number of channels as \mathbf{A} . And use the sigmoid function to activate the convolution result, constraining the value of weight vector $\mathbf{V} \in \mathbb{R}^{c \times 1 \times 1}$ between 0 and 1. Finally, we perform an outer product for \mathbf{X} and \mathbf{V} , and the result will add the initial feature $\mathbf{X} \in \mathbb{R}^{c \times h \times w}$ as a residual:

$$\mathbf{U} = \mathbf{X} \oplus \mathbf{X} \otimes Sigmoid[\Phi(\mathbf{A})] \quad (4)$$

Where \otimes denotes the Element-wise product, Φ denotes 1×1 convolution, and feature maps \mathbf{U} represent the output feature RGB' and Dep' . We use adaptive averaging instead of global averaging to more fully retain spatial position information depth features. The final output of the Pooling Attention Module:

$$\mathbf{P}'_i = RGB' \oplus Dep' \quad (5)$$

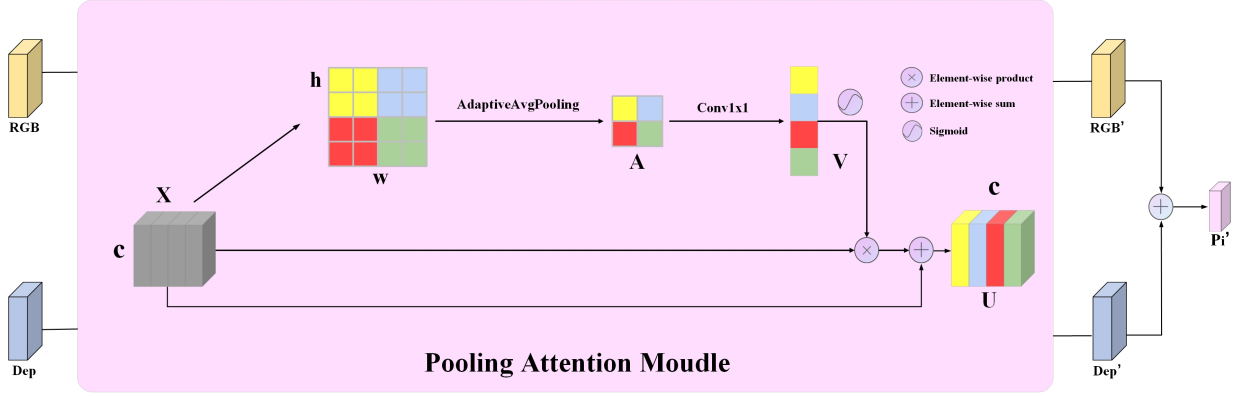


Figure 3: The details of the Pooling Attention Module. For each position (e.g., yellow), after applying adaptive average pooling, the pooled result A is obtained. Subsequently, through a 1×1 convolution and sigmoid activation function, constrain the value of weight vector V between 0 and 1. The output feature U is obtained by taking the weighted sum of the input feature X .

P'_i ($i \in [1,3]$) will act in the three-level decoder(decoder1-decoder3) during the upsampling process.

3.3 Multi-modal Interaction Module

When adjacent objects in an image exhibit similar appearances, it is difficult to distinguish their categories. Moreover, the influence of lighting variations and object occlusion, particularly in the corners of objects, can lead to their integration with the background. This makes it challenging to accurately identify the object's edges, resulting in misclassification of the object as part of the background. The depth information is not affected by lighting conditions and can accurately distinguish between objects and the background based on depth values. So, we designed the MIM module to complement depth information to RGB features. Meanwhile, it leverages RGB features to enhance the correlation between RGB and depth features.

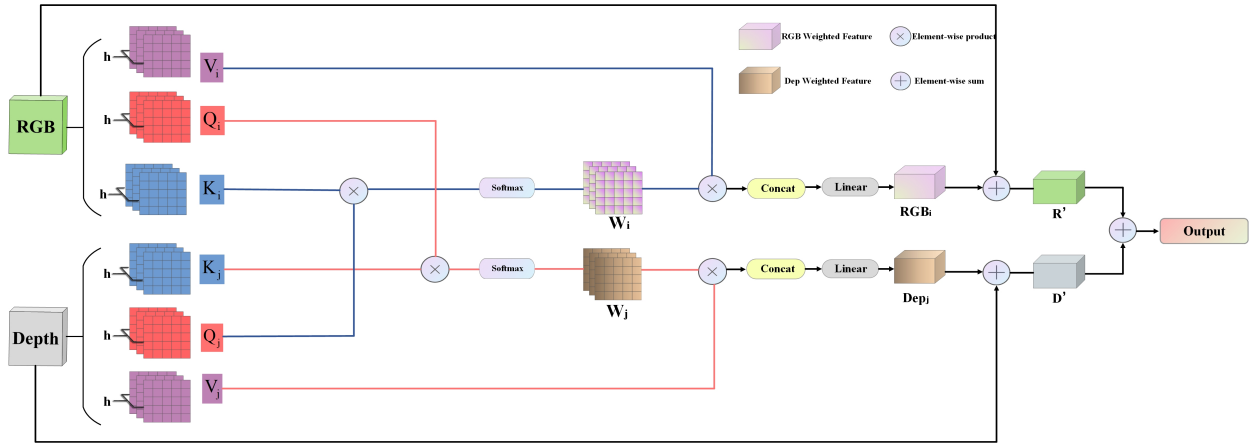


Figure 4: Multi-modal Interaction Module. The RGB feature and the depth feature are linearly transformed to obtain two sets of QKV (e.g., blue line) for multi-head attention, where h is the number of attention heads set to 8. The weighted summation of input features X_i^{RGB} and X_j^{Depth} yields R' and D' , which are then element-wise added to obtain the output result.

The Multi-modal Interaction Fusion Module achieves dual-mode feature fusion, as depicted in Fig. 4. Here, $X_i^{RGB} \in \mathbb{R}^{c \times h \times w}$ and $X_j^{Depth} \in \mathbb{R}^{c \times h \times w}$ correspond to the RGB feature and depth feature, respectively, extracted from the final layer output of ResNet encoder. The feature channels are denoted as 'c,' and their spatial dimensions are 'h x w.' First, the two feature maps are linearly mapped to generate multi-head query(Q), key(K), and value(V) vectors. Here, 'i' and

'j' represent the RGB and depth features, respectively. These linear mappings are accomplished via fully connected layers, where each attentional head possesses its unique weight matrix. For each attention head, We calculate the dot product between two sets of Q and K, and then normalize the results to a range between 0 and 1 using the softmax function to get the transmembrane state attention mask W_i and W_j :

$$W_i = \text{softmax}(Q_i K_j^T / \text{sqrt}(d_k)) \quad (6)$$

$$W_j = \text{softmax}(Q_j K_i^T / \text{sqrt}(d_k)) \quad (7)$$

Where W_i and W_j represent the RGB attention mask and the Depth attention mask, and d_k is the dimension of the vector. Then we calculate the RGB Weighted Feature RGB_i and the Dep Weighted Feature Dep_j . We obtain the final output features R' and D' through the use of a residual connection:

$$RGB_i = W_i \otimes V_i \quad (8)$$

$$R' = RGB_i \oplus X_i^{RGB} \quad (9)$$

Where RGB_i represent the RGB Weighted Feature, V_i represent the value vector from the RGB feature, multiplying with weight matrix W_i . R' represents the RGB features after the fusion with depth. Likewise:

$$Dep_j = W_j \otimes V_j \quad (10)$$

$$D' = Dep_j \oplus X_j^{Depth} \quad (11)$$

Where Dep_j represent the Depth Weighted Feature, V_j represent the value vector from the RGB feature, multiplying with weight matrix W_j . D' represents the Depth features after the fusion with RGB, \otimes represents the Element-wise product and \oplus represents the Element-wise sum.

3.4 Loss Function

In this paper, the network performs supervised learning on four different levels of decoding features. We employ nearest-neighbor interpolation to reduce the resolution of semantic labels. Additionally, 1x1 convolutions and Softmax functions are utilized to compute the classification probability for each pixel within the output features from the four upsample layers, respectively. The loss function \mathcal{L}_i of layer i is the pixel-level cross entropy loss:

$$\mathcal{L}_i = \frac{1}{N_i} \sum_{\forall p,q} -Y(p, q) \log(Y'(p, q)) \quad (12)$$

Where, N_i denote the number of pixels in layer i, p, q is the pixel position, Y' is the classification probability of the output, and Y is the label category. The final loss function \mathcal{L} of the network is obtained by summing the pixel-level loss functions of the four decoding layers:

$$\mathcal{L} = \sum_{i=1}^4 \mathcal{L}_i \quad (13)$$

By optimizing the above loss function, the network can get the final segmentation result after one training.

4 Experiment

4.1 Datasets and Evaluation Measures

NYU-Depth V2 [37] dataset is a widely used indoor scene understanding dataset for computer vision and deep learning research. It is an aggregation of video sequences from various indoor scenes recorded by RGB-D cameras from the Microsoft Kinect and is an updated version of the NYU-Depth dataset published by Nathan Silberman and Rob Fergus in 2011. It contains 1449 RGBD images, depth images, and semantic tags in the indoor environment. The dataset includes different indoor scenes, scene types, and unlabeled frames, and each object can be represented by a class and an instance number.

SUN RGB-D [38] dataset contains image samples from multiple scenes, covering various indoor scenes such as offices, bedrooms, and living rooms. It has 37 categories and contains 10335 RGBD images with pixel-level annotations, of which 5285 are used as training images and 5050 are used as test images. This special dataset is captured by four different sensors: Intel RealSense, Asus Xtion, Kinect v1, and v2. Besides, this densely annotated dataset includes

146,617 2D polygons, 64,595 3D bounding boxes with accurate object orientations, and a 3D room layout as well as an imaged-based scene category.

We evaluate the results using two standard metrics, Pixel Accuracy (Pixel Acc), and Mean Intersection Over Union (mIoU).

mIoU: Intersection over Union is a measure of semantic segmentation, where the intersection over Union ratio of a class is the ratio of the intersection over Union of its true labels and predicted values, while mIoU is the average intersection over Union ratio of each class in the dataset.

$$mIoU = \frac{1}{k+1} \sum_{i=0}^k \frac{p_{ij}}{\sum_{i=0}^k p_{ij} + \sum_{i=0}^k p_{ji} - p_{ii}}. \quad (14)$$

Where p_{ij} represents the predict i as j, and p_{ji} represents the predict j as i. p_{ii} means to predict the correct value. k represents the number of categories.

Acc: Pixel accuracy refers to pixel accuracy, which is the simplest metric that represents the proportion of correctly labelled pixels to the total number of pixels.

$$PA = \frac{\sum_{i=0}^k p_{ii}}{\sum_{i=0}^k \sum_{j=0}^k p_{ij}}. \quad (15)$$

Where p_{ii} means to predict the correct value, and p_{ij} means to predict i to j. k represents the number of categories.

4.2 Implementation Details

We implemented and trained our proposed network model using the PyTorch framework. To enhance the diversity of the training data, we applied random scaling and mirroring. Subsequently, all RGB and depth images were resized to 480×480 for network inputs, and semantic labels were adjusted to sizes of 480×480 , 240×240 , 120×120 , and 60×60 for deep supervision training. As the backbone for our encoder, we utilized a pre-trained ResNet50 [39] from the ImageNet classification dataset [40]. To refine the network structure, following [41, 42, 43], we adjust it by replacing the 7×7 convolution in the input stem with three consecutive 3×3 convolutions. The training process was conducted on an NVIDIA GeForce GTX 3090 GPU using stochastic gradient descent optimization. Parameters were set with a batch size of 6, an initial learning rate of 0.003, 500 epochs, and momentum and weight decay values of 0.9 and 0.0005, respectively.

4.3 Quantitative Results on NYUv2 and SUN RGB-D

Firstly, we compare the proposed method with the existing methods on the NYUv2 dataset. As shown in Table 1, we outperformed existing methods on mIoU and Acc metrics. Specifically, In our network with ResNet-50 as an encoder, the pixel Accuracy and average crossover ratio of semantic segmentation on the NYUv2 test set are 77.2% and 51.9%. For example, our method compared to RDFNet which also uses ResNet50, i.e. improved by 2.4% and 3.2% on Acc and mIoU, this indicates a significant enhancement in segmentation accuracy achieved by our MIPANet using the same ResNet50 architecture. Compared to

SGNet which uses ResNet101, i.e. improved by 1.6% and 2.3% on Acc and mIoU, our 50 floors are already superior to ResNet using 101 floors, this is because we have carefully designed the network structure and the multi-modal feature fusion module, and we achieved better segmentation results without the use of intense networks while reducing training time. Where R represent ResNet and ‘-’ means No Acc metrics were tested. We compared different network structures of different methods, specifically, ESANet consists of two ResNet18 as the Backbone, and ACNet consists of three ResNet50 as the Backbone.

Then we further compare the proposed algorithm with the existing algorithm on the SUN RGB-D dataset. As shown in Table 2, our method achieves a higher mIoU on the SUN RGB-D dataset compared to all other methods. For example, our MIPANet compared to SGNet, i.e. improved by 1.3% and 1.7% on Acc and mIoU. This indicates that our module can uphold superior segmentation accuracy even on the extensive SUN RGB-D dataset. For different Backbones, the performance of ResNet101 is generally higher than ResNet50, and the performance of ResNet50 is also generally higher than ResNet18. We chose ResNet50 as our backbone to achieve high performance while spending less training time compared to ResNet101. And the mIoU and Acc of our method on the two data sets increased by 4.5%,2.1% and 3.3%,1.2% compared with the baseline, as shown in the red part in the tables.

Table 1: MIPANet compared to the state-of-the-art methods on the NYUDv2 dataset.

Model	Method	Backbone	mIoU(%)	Pix.Acc(%)
ResNet18	ESANet[16]	2 x R18	48.2	-
ResNet50	RDFNet[7]	2 x R50	47.7	74.8
	ACNet[15]	3 x R50	48.3	-
	SA-Gate[44]	2 x R50	50.4	-
	ESANet	2 x R50	50.5	-
	DynMM[45]	R50	51.0	-
	RedNet[8]	2 x R50	47.2	-
	SGNet[46]	R101	49.6	75.6
ResNet101	RDFNet	2 x R101	49.1	75.6
	ShapeConv[47]	R101	51.3	76.4
	Baseline	2 x R50	47.4	75.1
ResNet50	Ours(MIPA)	2 x R50	51.9 (+ 4.5%)	77.2 (+ 2.1%)

Table 2: MIPANet compared to the state-of-the-art methods on the SUN RGB-D dataset.

Model	Method	Backbone	mIoU(%)	Pix.Acc(%)
ResNet34	EMSANet[48]	2 x R34	48.5	-
ResNet50	ACNet[15]	3 x R50	48.1	-
	ESANet[16]	2 x R50	48.3	-
	RedNet[8]	2 x R50	47.8	81.3
ResNet101	SGNet[46]	R101	47.1	81.0
	CANet[49]	R101	48.3	82.0
	CGBNet[50]	R101	48.2	82.3
	ShapeConv[47]	R101	48.6	82.2
ResNet152	RDFNet[7]	2 x R152	47.7	81.5
ResNet50	Baseline	2 x R50	45.5	81.1
	Ours(MIPA)	2 x R50	48.8 (+ 3.3%)	82.3 (+ 1.2%)

4.4 Visualization results on NYUv2

To more intuitively demonstrate the improvement of our method on the semantic segmentation task of indoor scenes, the visualization results of the network on the NYUv2 dataset are presented below.

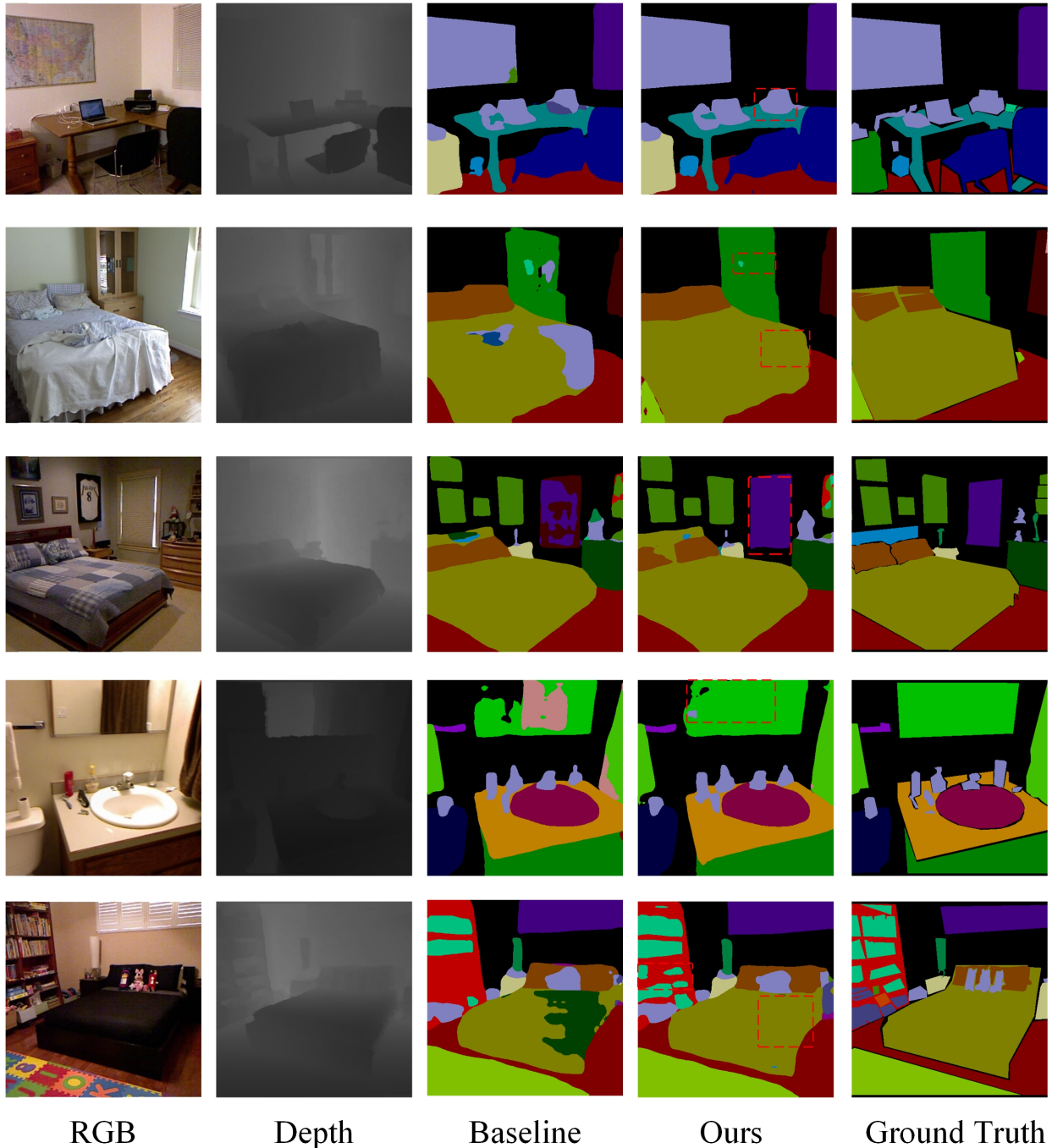


Figure 5: Visual result of MIPANet on NYUv2 dataset. The optimization effect is more pronounced in the red dotted box.

From the graph, it can be seen that our method has significantly improved the results compared to Baseline. As shown in the dashed box in the figure, due to the addition of depth information, our network can more accurately distinguish items from the background. For example, in the visualization results of the fourth image, for the mirror on the wall,

the baseline mistakenly treated it as a part of the background, and we used depth information to know that its distance information was different from the background, so we correctly classified it as a mirror. Fig. 5 shows the visualisation results of the proposed algorithm on the NYUv2 dataset. From left to right the columns represent the RGB image, the Depth image, the baseline model results with ResNet-50 backbone, MIPANet(Ours), and Ground Truth. It can be seen that the algorithm in this paper has achieved accurate segmentation results in various complex indoor scenes, and can better segment difficult-to-identify objects such as "carpet" and "book", and obtain finer edge segmentation results at the same time.

4.5 Ablation Study on PAM and MIM on NYUv2

We conducted ablation experiments between PAM and MIM on the NYUv2 dataset. Specifically, the RGB feature and depth feature input PAM to get RGB' and Dep', Due to the difference between the two modalities, we consider the parameter-sharing problem of PAM. In addition, We consider the effect of network depth on information interaction, so we use MIM in both layer 3 and layer 4 of the encoder. Fig. 6 shows the results of PAM and MIM ablation studies on the NYUv2 dataset. B1-B4 denote the different settings of PAM and MIM: B1 (PAM without shared parameters and MIM used on ResNet Layer4), B2 (PAM with shared parameters and MIM used on ResNet Layer4), B3 (PAM without shared parameters and MIM used on ResNet Layer3 and Layer4), B4 (PAM with shared parameters and MIM used on ResNet Layer3 and Layer4). It can be seen that PAM without shared parameters and MIM is only used in the last layer of the encoder to achieve the best results, with the highest mIoU of 51.9%.

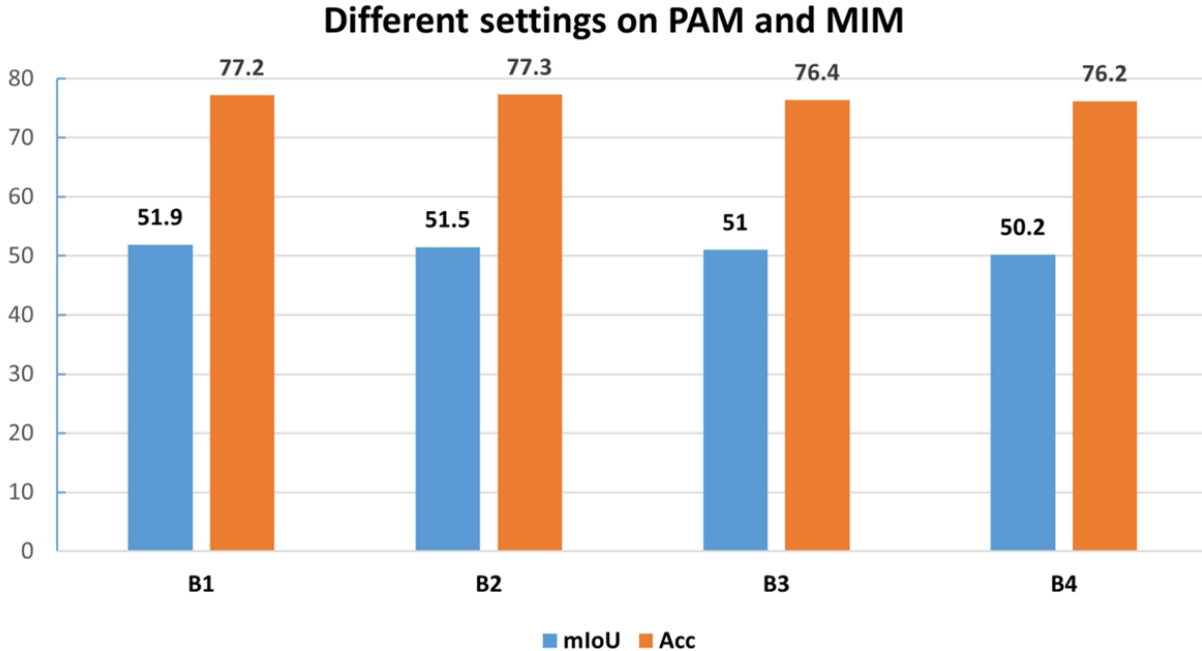


Figure 6: Ablation Study on PAM and MIM. When set to B1, the best segmentation result is 51.9%

4.6 Ablation Study on NYUv2 and SUN-RGBD

To study the influence of different modules on the segmentation performance, we conducted ablation experiments on NYUv2 and SUN-RGBD. '✓' indicates the use of this module and '✗' indicates that the module is not used. For example, our PAM module achieved a superiority of 1.5% and 0.9% over the baseline in terms of mIoU and Acc indicators, respectively. Our MIM module also achieved a superiority of 3.7% and 1.9% over the baseline in terms of mIoU and Acc indicators. This suggests that each of the proposed modules can be employed independently to enhance segmentation accuracy.

It can be seen that our Module outperforms the Baseline in fusing cross-modal features and achieving better results on both datasets. By utilizing both PAM and MIM modules, we achieved the highest 51.9% mIoU on the NYUv2 dataset

Table 3: Ablation studies on NYUDv2 and SUN-RGBD dataset for PAM and MIM

Method	PAM	MIM	NYUv-2		SUN-RGBD	
			mIoU(%)	Acc(%)	mIoU(%)	Acc(%)
Baseline	✗	✗	47.4	75.1	45.5	81.1
Ours	✓	✗	48.9	76.0	47.9	81.3
	✗	✓	51.1	77.0	48.3	81.5
	✓	✓	51.9	77.2	48.8	82.3

and the highest 48.8% mIoU on the SUN RGB-D dataset. This demonstrates that our two designed modules can be jointly optimized to enhance segmentation accuracy collaboratively.

5 Conclusions

In this paper, we tackle a fundamental challenge in indoor RGB-D semantic segmentation—efficiently fusing features from two distinct modes. We designed an innovative Multi-modal Interaction and Pooling Attention network, which uses a small and flexible PAM module in the shallow layer of the network to enhance the feature extraction capability of the network, and uses an MIM module in the last layer of the network to effectively integrate RGB features and depth features. We use the complementary information between RGB and depth mode to improve the accuracy of semantic segmentation in indoor scenes. In future work, we will extend our method to enhance its generalization ability in RGB-D semantic segmentation. Furthermore, we anticipate performance improvements by integrating tasks such as depth estimation into the existing framework, facilitating collaborative interactions between networks.

limitation. Our method’s effectiveness has been exclusively validated on CNN networks, but we haven’t conducted verification on other network architectures, such as Transformer. In addition, during the segmentation verification on the test set, the requirement to input both RGB and depth images limits the network’s generalization ability. Consequently, the network may not achieve optimal segmentation results for datasets lacking depth information.

References

- [1] J. Long, E. Shelhamer, and T. Darrell, “Fully convolutional networks for semantic segmentation,” in *Proceedings of the IEEE conference on computer vision and pattern recognition*, pp. 3431–3440, 2015.
- [2] M. Li, M. Wei, X. He, and F. Shen, “Enhancing part features via contrastive attention module for vehicle re-identification,” in *2022 IEEE International Conference on Image Processing (ICIP)*, pp. 1816–1820, IEEE, 2022.
- [3] Z. Zhang, “Microsoft kinect sensor and its effect,” *IEEE multimedia*, vol. 19, no. 2, pp. 4–10, 2012.
- [4] Y. He, W.-C. Chiu, M. Keuper, and M. Fritz, “Std2p: Rgb-d semantic segmentation using spatio-temporal data-driven pooling,” in *Proceedings of the IEEE conference on computer vision and pattern recognition*, pp. 4837–4846, 2017.
- [5] C. Couprie, C. Farabet, L. Najman, and Y. LeCun, “Indoor semantic segmentation using depth information,” *arXiv preprint arXiv:1301.3572*, 2013.
- [6] S. Gupta, R. Girshick, P. Arbeláez, and J. Malik, “Learning rich features from rgb-d images for object detection and segmentation,” in *Computer Vision—ECCV 2014: 13th European Conference, Zurich, Switzerland, September 6–12, 2014, Proceedings, Part VII 13*, pp. 345–360, Springer, 2014.
- [7] S.-J. Park, K.-S. Hong, and S. Lee, “Rdfnet: Rgb-d multi-level residual feature fusion for indoor semantic segmentation,” in *Proceedings of the IEEE international conference on computer vision*, pp. 4980–4989, 2017.
- [8] J. Jiang, L. Zheng, F. Luo, and Z. Zhang, “Rednet: Residual encoder-decoder network for indoor rgb-d semantic segmentation,” *arXiv preprint arXiv:1806.01054*, 2018.

- [9] D. Eigen and R. Fergus, “Predicting depth, surface normals and semantic labels with a common multi-scale convolutional architecture,” in *Proceedings of the IEEE international conference on computer vision*, pp. 2650–2658, 2015.
- [10] A. Wang, J. Lu, G. Wang, J. Cai, and T.-J. Cham, “Multi-modal unsupervised feature learning for rgb-d scene labeling,” in *Computer Vision—ECCV 2014: 13th European Conference, Zurich, Switzerland, September 6-12, 2014, Proceedings, Part V 13*, pp. 453–467, Springer, 2014.
- [11] F. Liu, C. Shen, and G. Lin, “Deep convolutional neural fields for depth estimation from a single image,” in *Proceedings of the IEEE conference on computer vision and pattern recognition*, pp. 5162–5170, 2015.
- [12] J. Hu, Z. Huang, F. Shen, D. He, and Q. Xian, “A bag of tricks for fine-grained roof extraction,” in *IGARSS 2023-2023 IEEE International Geoscience and Remote Sensing Symposium*, IEEE, 2023.
- [13] J. Hu, Z. Huang, F. Shen, D. He, and Q. Xian, “A robust method for roof extraction and height estimation,” in *IGARSS 2023-2023 IEEE International Geoscience and Remote Sensing Symposium*, IEEE, 2023.
- [14] C. Hazirbas, L. Ma, C. Domokos, and D. Cremers, “Fusenet: Incorporating depth into semantic segmentation via fusion-based cnn architecture,” in *Computer Vision—ACCV 2016: 13th Asian Conference on Computer Vision, Taipei, Taiwan, November 20-24, 2016, Revised Selected Papers, Part I 13*, pp. 213–228, Springer, 2017.
- [15] X. Hu, K. Yang, L. Fei, and K. Wang, “Acnet: Attention based network to exploit complementary features for rgbd semantic segmentation,” in *2019 IEEE International Conference on Image Processing (ICIP)*, pp. 1440–1444, IEEE, 2019.
- [16] D. Seichter, M. Köhler, B. Lewandowski, T. Wengefeld, and H.-M. Gross, “Efficient rgb-d semantic segmentation for indoor scene analysis,” in *2021 IEEE international conference on robotics and automation (ICRA)*, pp. 13525–13531, IEEE, 2021.
- [17] A. Vaswani, N. Shazeer, N. Parmar, J. Uszkoreit, L. Jones, A. N. Gomez, Ł. Kaiser, and I. Polosukhin, “Attention is all you need,” *Advances in neural information processing systems*, vol. 30, 2017.
- [18] F. Shen, M. Wei, and J. Ren, “Hsgnet: Object re-identification with hierarchical similarity graph network,” *arXiv preprint arXiv:2211.05486*, 2022.
- [19] J. Fu, J. Liu, H. Tian, Y. Li, Y. Bao, Z. Fang, and H. Lu, “Dual attention network for scene segmentation,” in *Proceedings of the IEEE/CVF conference on computer vision and pattern recognition*, pp. 3146–3154, 2019.
- [20] F. Shen, J. Zhu, X. Zhu, J. Huang, H. Zeng, Z. Lei, and C. Cai, “An efficient multiresolution network for vehicle reidentification,” *IEEE Internet of Things Journal*, vol. 9, no. 11, pp. 9049–9059, 2021.
- [21] F. Shen, X. Peng, L. Wang, X. Zhang, M. Shu, and Y. Wang, “Hsgm: A hierarchical similarity graph module for object re-identification,” in *2022 IEEE International Conference on Multimedia and Expo (ICME)*, pp. 1–6, IEEE, 2022.
- [22] S. Woo, J. Park, J.-Y. Lee, and I. S. Kweon, “Cbam: Convolutional block attention module,” in *Proceedings of the European conference on computer vision (ECCV)*, pp. 3–19, 2018.
- [23] F. Wang, M. Jiang, C. Qian, S. Yang, C. Li, H. Zhang, X. Wang, and X. Tang, “Residual attention network for image classification,” in *Proceedings of the IEEE conference on computer vision and pattern recognition*, pp. 3156–3164, 2017.
- [24] J. Hu, L. Shen, and G. Sun, “Squeeze-and-excitation networks,” in *Proceedings of the IEEE conference on computer vision and pattern recognition*, pp. 7132–7141, 2018.
- [25] Q. Wang, B. Wu, P. Zhu, P. Li, W. Zuo, and Q. Hu, “Eca-net: Efficient channel attention for deep convolutional neural networks,” in *Proceedings of the IEEE/CVF conference on computer vision and pattern recognition*, pp. 11534–11542, 2020.
- [26] C. Qiao, F. Shen, X. Wang, R. Wang, F. Cao, S. Zhao, and C. Li, “A novel multi-frequency coordinated module for sar ship detection,” in *2022 IEEE 34th International Conference on Tools with Artificial Intelligence (ICTAI)*, pp. 804–811, IEEE, 2022.
- [27] Z. Huang, X. Wang, L. Huang, C. Huang, Y. Wei, and W. Liu, “Ccnet: Criss-cross attention for semantic segmentation,” in *Proceedings of the IEEE/CVF international conference on computer vision*, pp. 603–612, 2019.
- [28] Q. Ha, K. Watanabe, T. Karasawa, Y. Ushiku, and T. Harada, “Mfnet: Towards real-time semantic segmentation for autonomous vehicles with multi-spectral scenes,” in *2017 IEEE/RSJ International Conference on Intelligent Robots and Systems (IROS)*, pp. 5108–5115, IEEE, 2017.
- [29] F. Shen, X. Du, L. Zhang, and J. Tang, “Triplet contrastive learning for unsupervised vehicle re-identification,” *arXiv preprint arXiv:2301.09498*, 2023.

- [30] Q. Zhang, S. Zhao, Y. Luo, D. Zhang, N. Huang, and J. Han, “Abmdrnet: Adaptive-weighted bi-directional modality difference reduction network for rgb-t semantic segmentation,” in *Proceedings of the IEEE/CVF Conference on Computer Vision and Pattern Recognition*, pp. 2633–2642, 2021.
- [31] F. Shen, X. Shu, X. Du, and J. Tang, “Pedestrian-specific bipartite-aware similarity learning for text-based person retrieval,” in *Proceedings of the 31th ACM International Conference on Multimedia*, 2023.
- [32] Y. Sun, W. Zuo, and M. Liu, “Rtfnnet: Rgb-thermal fusion network for semantic segmentation of urban scenes,” *IEEE Robotics and Automation Letters*, vol. 4, no. 3, pp. 2576–2583, 2019.
- [33] K. Xiang, K. Yang, and K. Wang, “Polarization-driven semantic segmentation via efficient attention-bridged fusion,” *Optics Express*, vol. 29, no. 4, pp. 4802–4820, 2021.
- [34] F. Shen, J. Zhu, X. Zhu, Y. Xie, and J. Huang, “Exploring spatial significance via hybrid pyramidal graph network for vehicle re-identification,” *IEEE Transactions on Intelligent Transportation Systems*, vol. 23, no. 7, pp. 8793–8804, 2021.
- [35] F. Shen, Y. Xie, J. Zhu, X. Zhu, and H. Zeng, “Git: Graph interactive transformer for vehicle re-identification,” *IEEE Transactions on Image Processing*, 2023.
- [36] Z. Zhuang, R. Li, K. Jia, Q. Wang, Y. Li, and M. Tan, “Perception-aware multi-sensor fusion for 3d lidar semantic segmentation,” in *Proceedings of the IEEE/CVF International Conference on Computer Vision*, pp. 16280–16290, 2021.
- [37] N. Silberman, D. Hoiem, P. Kohli, and R. Fergus, “Indoor segmentation and support inference from rgb-d images,” in *Computer Vision—ECCV 2012: 12th European Conference on Computer Vision, Florence, Italy, October 7–13, 2012, Proceedings, Part V 12*, pp. 746–760, Springer, 2012.
- [38] S. Song, S. P. Lichtenberg, and J. Xiao, “Sun rgb-d: A rgb-d scene understanding benchmark suite,” in *Proceedings of the IEEE conference on computer vision and pattern recognition*, pp. 567–576, 2015.
- [39] K. He, X. Zhang, S. Ren, and J. Sun, “Deep residual learning for image recognition,” in *Proceedings of the IEEE conference on computer vision and pattern recognition*, pp. 770–778, 2016.
- [40] O. Russakovsky, J. Deng, H. Su, J. Krause, S. Satheesh, S. Ma, Z. Huang, A. Karpathy, A. Khosla, M. Bernstein, et al., “Imagenet large scale visual recognition challenge,” *International journal of computer vision*, vol. 115, pp. 211–252, 2015.
- [41] X. Fu, F. Shen, X. Du, and Z. Li, “Bag of tricks for “vision meet alage” object detection challenge,” in *2022 6th International Conference on Universal Village (UV)*, pp. 1–4, IEEE, 2022.
- [42] F. Shen, X. He, M. Wei, and Y. Xie, “A competitive method to vipriors object detection challenge,” *arXiv preprint arXiv:2104.09059*, 2021.
- [43] F. Shen, Z. Wang, Z. Wang, X. Fu, J. Chen, X. Du, and J. Tang, “A competitive method for dog nose-print re-identification,” *arXiv preprint arXiv:2205.15934*, 2022.
- [44] X. Chen, K.-Y. Lin, J. Wang, W. Wu, C. Qian, H. Li, and G. Zeng, “Bi-directional cross-modality feature propagation with separation-and-aggregation gate for rgb-d semantic segmentation,” in *European Conference on Computer Vision*, pp. 561–577, Springer, 2020.
- [45] Z. Xue and R. Marculescu, “Dynamic multimodal fusion,” in *Proceedings of the IEEE/CVF Conference on Computer Vision and Pattern Recognition*, pp. 2574–2583, 2023.
- [46] L.-Z. Chen, Z. Lin, Z. Wang, Y.-L. Yang, and M.-M. Cheng, “Spatial information guided convolution for real-time rgb-d semantic segmentation,” *IEEE Transactions on Image Processing*, vol. 30, pp. 2313–2324, 2021.
- [47] J. Cao, H. Leng, D. Lischinski, D. Cohen-Or, C. Tu, and Y. Li, “Shapeconv: Shape-aware convolutional layer for indoor rgb-d semantic segmentation,” in *Proceedings of the IEEE/CVF international conference on computer vision*, pp. 7088–7097, 2021.
- [48] D. Seichter, S. B. Fishedick, M. Köhler, and H.-M. Groß, “Efficient multi-task rgb-d scene analysis for indoor environments,” in *2022 International Joint Conference on Neural Networks (IJCNN)*, pp. 1–10, IEEE, 2022.
- [49] Q. Tang, F. Liu, T. Zhang, J. Jiang, and Y. Zhang, “Attention-guided chained context aggregation for semantic segmentation,” *Image and Vision Computing*, vol. 115, p. 104309, 2021.
- [50] H. Ding, X. Jiang, B. Shuai, A. Q. Liu, and G. Wang, “Semantic segmentation with context encoding and multi-path decoding,” *IEEE Transactions on Image Processing*, vol. 29, pp. 3520–3533, 2020.